

# Recent oppositely directed trends in solar climate forcings and the global mean surface air temperature. II. Different reconstructions of the total solar irradiance variation and dependence on response time scale

BY MIKE LOCKWOOD<sup>1,2,\*</sup> AND CLAU FRÖHLICH<sup>3</sup>

<sup>1</sup>*Space Environment Physics Group, School of Physics and Astronomy, University of Southampton, Southampton SO17 1BJ, Hampshire, UK*

<sup>2</sup>*Rutherford Appleton Laboratory, Chilton OX11 0QX, Oxfordshire, UK*

<sup>3</sup>*Physikalisch-Meteorologisches Observatorium Davos, World Radiation Center, 7260 Davos Dorf, Switzerland*

We have previously placed the solar contribution to recent global warming in context using observations and without recourse to climate models. It was shown that all solar forcings of climate have declined since 1987. The present paper extends that analysis to include the effects of the various time constants with which the Earth's climate system might react to solar forcing. The solar input waveform over the past 100 years is defined using observed and inferred galactic cosmic ray fluxes, valid for either a direct effect of cosmic rays on climate or an effect via their known correlation with total solar irradiance (TSI), or for a combination of the two. The implications, and the relative merits, of the various TSI composite data series are discussed and independent tests reveal that the PMOD composite used in our previous paper is the most realistic. Use of the ACRIM composite, which shows a rise in TSI over recent decades, is shown to be inconsistent with most published evidence for solar influences on pre-industrial climate. The conclusions of our previous paper, that solar forcing has declined over the past 20 years while surface air temperatures have continued to rise, are shown to apply for the full range of potential time constants for the climate response to the variations in the solar forcings.

**Keywords:** solar variability; climate change; solar-terrestrial physics

## 1. Introduction

In a recent paper (Lockwood & Fröhlich 2007—hereafter ‘paper 1’), we analysed the trends in both global air surface temperature anomaly data and observations of the various solar outputs, which have been proposed as contributors to global climate change over recent decades. It was shown that the changes in the Sun since 1987 have been in the wrong direction to contribute to the observed

\* Author and address for correspondence: Rutherford Appleton Laboratory, Chilton OX11 0QX, Oxfordshire, UK (m.lockwood@rl.ac.uk).

increase in the mean surface air temperature. In the present paper, we confirm this finding and show it does not depend on the assumed response time constant of the climate system. An accompanying paper (Lockwood in press—hereafter ‘paper 3’) will quantify the various contributions to the observed increase in the mean surface air temperature with derivation of, and allowance for, the relevant time constants for each contribution.

Paper 1 presented a review of evidence for a link between solar variations and pre-industrial climate, summarized some detection–attribution studies that detected a solar influence as late as the early part of the last century and showed that solar trends for the last 20 years have been in the wrong direction to have contributed to the continuing long-term rise in global air surface temperature. Contrary to the argument presented by Svensmark & Friis-Christensen (2007), this does not imply that paper 1 argued that the mechanisms that caused any solar variability effects on climate have somehow ceased at some point in the twentieth century, rather paper 1 found that they have simply been swamped by other factors in recent years.

Claims that the trend in the global mean surface air temperature is not still upward (e.g. D’Aleo 2007; Svensmark & Friis-Christensen 2007) are grossly misleading and ignore the great variability about the trend that has always been present. Such claims usually make use of the fact that 1998 gave the highest global mean air surface temperature anomaly observed to date. As will be discussed in paper 3, 1998 gave (like all recent years) high positive temperature anomaly values, but the reason why this particular year showed higher values than other recent years is that it contained an exceptional El Niño event that brought large amounts of energy from the sub-surface equatorial Pacific to the surface. El Niño years are peaks of the El Niño Southern Oscillation (ENSO) cycle and in the converse La Niña years of this oscillation, this warming effect turns to a cooling. Owing to natural climate variability (e.g. the difference between El Niño and La Niña years), one cannot accurately define a meaningful long-term trend by selecting specific start and end dates that happen to suit one’s argument. For example, if one selects 1998–2006, the temperature change is indeed downward, if one selects either 1997–2006 or 1999–2006, it is upward. Paper 1 employed running means over 7–13 years (and over the solar cycle length,  $L$ ) to determine the trend in the global mean air surface temperature and it has remained upward since 1987, when the trends in the solar data, evaluated using exactly the same procedure, gave declining solar forcing.

It has been pointed out (D’Aleo 2007) that paper 1 did not specifically consider the solar flare analysis of Scafetta & West (2003, 2006). This is true but not of great relevance because paper 1 did consider the change in the total solar irradiance (TSI) and Scafetta and West use flare occurrence rate only as a way of reconstructing TSI variations (useful before the time when direct space-based observations of TSI became available). Hence, the flares are used in their papers as a proxy indicator of TSI variations, and these authors make no suggestions that the flares themselves are an important contributor to the Earth’s climate. The explanation as to why the conclusions of paper 1 about the solar contribution in recent decades differ so markedly from those of Scafetta and West lies in the difference, as highlighted by Lean (2006), between the ACRIM composite of TSI observations (Willson 1997; Willson & Mordvinov 2003) and the PMOD composite (Fröhlich & Lean 2004; Fröhlich 2006); paper 1 employed

the PMOD whereas Scafetta and West used the ACRIM. In §2 of the present paper, we look at the implications of the various TSI data composites and discuss independent tests of their relative merits.

It has also been noted that the procedure for smoothing out the solar cycle variation that was employed in [paper 1](#) introduces some ‘precognition’—in that the raw data for a time  $(x+L/2)$  (where  $L$  is the solar cycle length) can influence the smoothed data for the time  $x$  ([D’Aleo 2007](#)). This is undoubtedly true and this is why the global mean air surface temperature anomaly in [paper 1](#) was processed in exactly the same way as the solar data. Hence, the adoption of this procedure to estimate trends does not account for the difference in the solar and temperature trends in any way. However, the use of such smoothing does introduce another factor. In [paper 1](#), we completely removed the solar cycle variations to reveal the long-term trends. The actual response of the climate system may not have as long a time constant as the procedure adopted in [paper 1](#). Indeed, as discussed in §3 of the present paper and in [paper 3](#), the fact that solar cycle variations are not completely damped out tells us that this is not the whole story. The key unknown is how deeply into the Earth’s oceans a given variation penetrates. If it penetrates sufficiently deeply, the large thermal capacity of the part of the ocean involved would mean that the time constant was extremely long ([Wigley & Raper 1990](#)); in such a case, the analysis of long-term trends given in [paper 1](#) would be adequate to fully describe the Earth’s response to solar variations. However, the recent studies suggest that the sunspot cycle variations in solar forcing, in particular, do not penetrate very deeply into the oceans and so the time constant is smaller; this means that solar cycle variations are not completely suppressed. For example, [Douglass \*et al.\* \(2004\)](#) report a response time to solar variations of  $\tau < 1$  year and, recently, [Schwartz \(2007\)](#) reports an overall time constant (for all forcings and responses) of  $\tau = 5 \pm 1$  years. In §3, we show that this uncertainty in the response time constant does not influence our conclusion in [paper 1](#) that the upward trend in global mean air surface temperature cannot be ascribed to solar variations. In [paper 3](#), the relative contributions of solar variations, ocean–atmosphere energy exchange, volcanic effects and an upward linear trend (to account for anthropogenic emissions of greenhouse gases and aerosols) are quantified. Such multivariate fit analyses have been presented several times previously, but this new analysis allows the time constants of the responses to each of these forcings to be accounted for, and fitted, individually.

## 2. TSI composites

[Paper 1](#) employed the composite TSI data series compiled by PMOD, Davos ([Fröhlich 2000, 2006](#); [Fröhlich & Lean 2004](#)). Compilation of a composite is necessary because TSI monitors have been operated for only limited intervals; compilation of a continuous homogeneous data sequence, which can reveal the true long-term trend, has therefore required the use of data from several different instruments. This means that the intercalibration of those instruments, and how it changes with time as the instruments degrade, is a key issue in the compilation of such a composite. The development of the PMOD composite is well documented in the literature by the series of papers from [Fröhlich & Lean \(1998\)](#) to [Fröhlich \(2000, 2003, 2006\)](#).

Apart from the PMOD composite, there are two others published: the ACRIM composite (Willson 1997; Willson & Mordvinov 2003) and the IRMB composite (Dewitte *et al.* 2004). All three use the time series of data from the HF instrument on Nimbus 7 and the ACRIM-I and ACRIM-II instruments until early 1996. For later times, the ACRIM composite continues to use ACRIM-II supplemented by ACRIM-III, whereas PMOD and IRMB use different combinations of data from the VIRGO instrument on the SoHO spacecraft (Fröhlich *et al.* 1995). VIRGO has two active cavity radiometers, called PMO6-V and the dual absolute radiometer (DIARAD). (For details about all the time series used, see the original publications cited here.) Besides the different data used during cycle 23, the main difference between the composites is the way the data are combined. Moreover, only the PMOD composite has applied corrections to HF and the ACRIM data, based on detailed studies of the long-term behaviour of the radiometers in space.

The three composites are shown in figure 1. In each case, the coloured lines give the daily values and the black line the 81-day running means. The colours used for the daily data show which instrument is used in which interval. Running means are taken over 81-day intervals because they cover three solar rotations (as seen from Earth) and very few patches of enhanced or decreased surface intensity (sunspot groups and patches of faculae, respectively) persist for a longer duration than this. The IRMB composite is constructed by first referring all datasets to space absolute radiometric reference (SARR; Crommelynck *et al.* 1995): for the ACRIM-II, ERBE/ERBS and VIRGO radiometers the adjustment is based on direct comparison; for the HF and ACRIM-I the calibration is traced back using ERBE/ERBS. During the time when VIRGO data are available, the PMOD and IRMB composites differ because the IRMB uses only the measurements of DIARAD, which allows one to correct only for changes due to the instrument exposure to solar radiation. One cannot also correct for the increase of sensitivity that is not exposure dependent and is manifested by comparisons of data from PMO6-V, ACRIM-II and ACRIM-III, and ERBS/ERBE. The PMOD composite uses the official SoHO VIRGO TSI dataset, which is a combination of the results of PMO6-V and DIARAD, corrected for the sensitivity increase as well as the effect of instrument exposure.

Figure 2 shows the differences between  $TSI_{ACRIM}$  (figure 2a) and  $TSI_{IRMB}$  (figure 2b), relative to  $TSI_{PMOD}$ , with the grey line giving daily values and the black line the 81-day running means. Two major features can be seen. The first is the rapid drift in calibration between  $TSI_{PMOD}$  and both  $TSI_{ACRIM}$  and  $TSI_{IRMB}$  before 1981. This arises because all three composites employ the Nimbus HF data for this interval, but ACRIM and IRMB have not employed the re-evaluation of the early degradation of the HF instrument that has been implemented in the PMOD. The second major difference is a near step-function change within what is termed the ‘ACRIM gap’. This is the interval between the loss of the ACRIM-I instrument in mid-1989 and the start of the ACRIM-II data late in 1991. All composites have to return to using the Nimbus HF data for this interval. The fact that the daily (grey line) and monthly (black line) differences are the same for  $(TSI_{ACRIM} - TSI_{PMOD})$  in and around the ACRIM gap is because the two composites make use of the same data series at this time and only differ in the (time-dependent) calibrations employed. The IRMB composite uses averages of the HF and ACRIM data. The HF data series has many sudden jumps that are

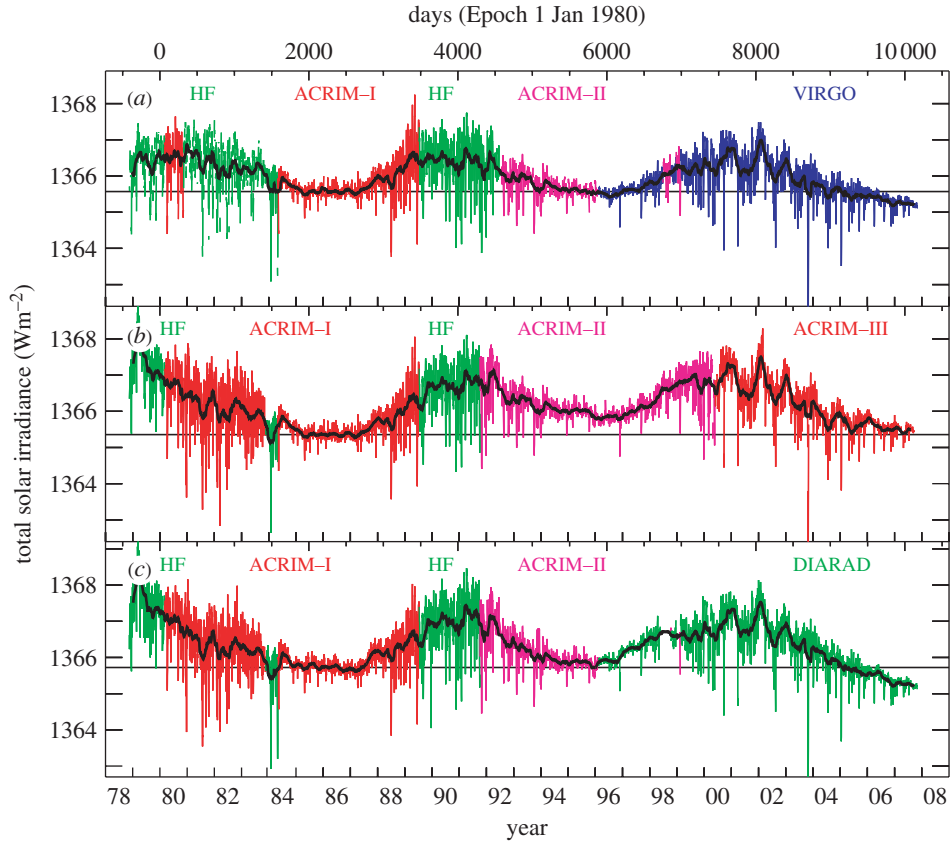


Figure 1. The (a) PMOD, (b) ACRIM and (c) IRMB composites of TSI (respectively,  $TSI_{PMOD}$ ,  $TSI_{ACRIM}$  and  $TSI_{IRMB}$ ). In (a–c) the coloured lines give daily values, with the colour giving the instrument yielding the data used. The thick black lines are 81-day running means and horizontal black lines are drawn through the mean for 1986 (the minimum between solar cycles 21 and 22) to highlight the trends in minimum values of the composites. For each panel, the lower horizontal scale gives the year and the upper scale the day number, where day 1 is 1 January 1980.

attributed to changes in the orientation of the spacecraft and to switch-offs (Kerr 1997; Fröhlich 2000). The horizontal lines in figure 2 give the differences for 1986, just before the ACRIM gap, and allow one to compare the evolution of the two sets of differences (Note that the same date is used to give reference levels in figure 1). The step-function change in the difference between  $TSI_{ACRIM}$  and  $TSI_{PMOD}$  arises because the PMOD makes allowance for a jump in the ACRIM gap and the ACRIM does not (see also Kerr 1997). Lee *et al.* (1995) and Chapman *et al.* (1996) drew attention to the existence of this and other calibration ‘glitches’ in the HF data by comparison with the ERBE TSI data and using models based on direct photometric observations of sunspots and faculae. The more detailed analysis of Fröhlich (2000) presents evidence for the reality of this jump. Other such jumps are known to have been caused by orientation changes and/or switching-off, because we can compare the HF data with ACRIM data for intervals when both are available. Figure 2a shows that it is the inclusion of an allowance for a glitch in the calibration of the HF data during the

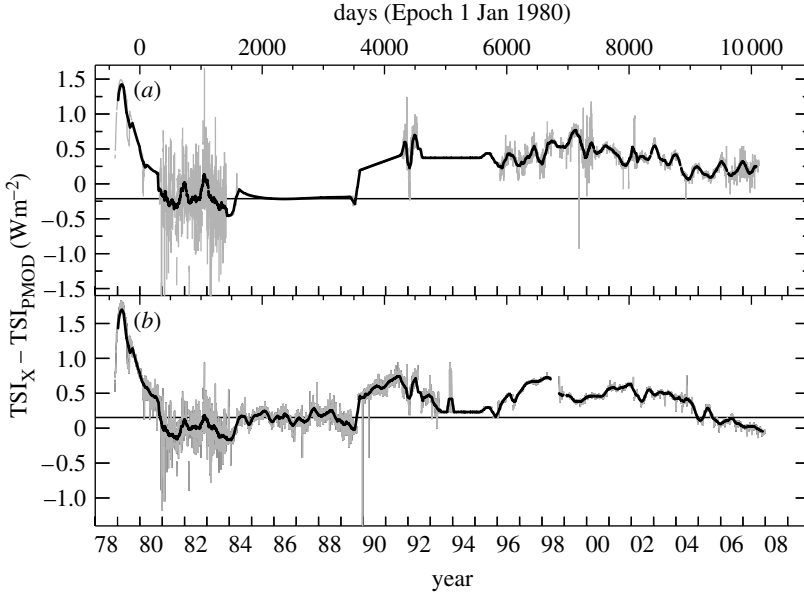


Figure 2. The difference between the (a) ACRIM and (b) IRMB composites relative to the PMOD of TSI ( $TSI_X - TSI_{PMOD}$ ). The grey line gives daily values and the black line shows 81-day running means. In several intervals the grey line is hidden behind the black line because the two composites employ data from the same instruments but the difference is non-zero as they apply different (time-dependent) calibrations. The horizontal line indicates the value of the difference during the solar minimum in 1986. During the time of the VIRGO/SoHO measurements, the ACRIM composite shows a only small trend (with respect to the PMOD), whereas the IRMB shows peak-to-peak deviations from the VIRGO TSI of approximately  $0.5 \text{ W m}^{-2}$ , which is about half the amplitude of the solar cycle variation. The step in the ACRIM gap during 1989 is clearly seen in both panels and is also by about half the amplitude of the solar cycle variation.

ACRIM gap in the PMOD composite, but not in the ACRIM, that is responsible for virtually all of the difference between the long-term drifts of the composites; the glitch in the ACRIM gap causes a rise in  $(TSI_{ACRIM} - TSI_{PMOD})$  of  $0.475 \text{ W m}^{-2}$  (from figure 1, this is approximately half the amplitude of the solar cycle variation), and this is almost exactly the same as the difference between these two composites by the end of the interval shown. (Note that there are other, smaller, rises and falls of this difference in figure 2a but they cancel out).

Figure 2b shows that the IRMB composite also fails to allow for the glitch during the ACRIM gap as the same step-function change can be seen in figure 2b during the ACRIM gap as in figure 2a. However, this step-like rise in  $(TSI_{IRMB} - TSI_{PMOD})$  is followed by a decline, a rise and then a gradual decline (oscillations that are of amplitude approximately half that of the solar cycle variation), such that by the end of the interval  $(TSI_{IRMB} - TSI_{PMOD})$  is below the 1986 level and near zero.

To analyse this intercalibration issue in relation to the biggest persistent difference in figure 2 (namely that in  $TSI_{ACRIM} - TSI_{PMOD}$ ), figure 3 presents a scatter plot of the daily values (in grey) and of (independent) 81-day means (in black) of  $TSI_{ACRIM}$  as a function of the simultaneous  $TSI_{PMOD}$  value. In addition to the main population, for which  $TSI_{ACRIM}$  consistently exceeds  $TSI_{PMOD}$  by a small amount, a second series of data points is seen forming a line

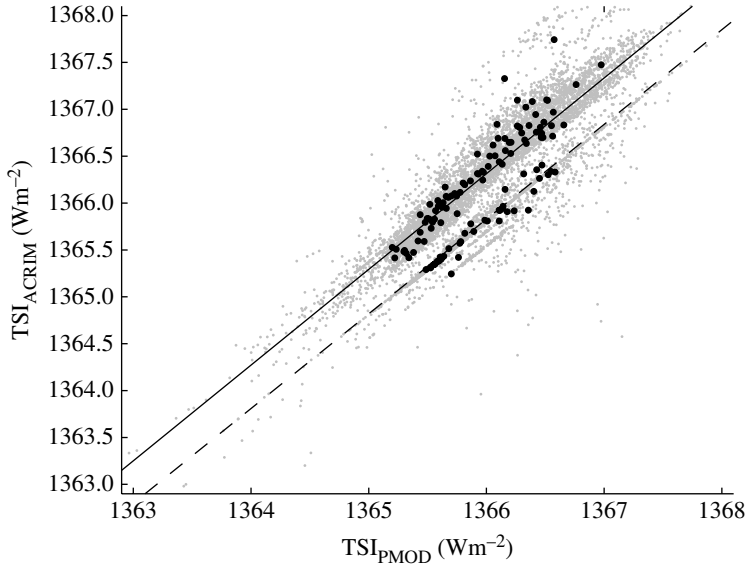


Figure 3. Scatter plot of the daily values (grey) and independent 81-day means (black) of  $TSI_{ACRIM}$  as a function of the corresponding  $TSI_{PMOD}$  value.

for which  $TSI_{ACRIM}$  is very close to, but very slightly smaller than  $TSI_{PMOD}$ ; these data points all originate from immediately before the glitch in the HF data during the ACRIM gap allowed for by the PMOD but not the ACRIM. The offset between this line and the best least-squares linear regression fit to the remaining points is  $0.57 \text{ W m}^{-2}$ . Note that all linear regressions shown in this paper allow for uncertainties in both parameters of the scatter plot by minimizing the r.m.s. length of the perpendiculars to the regression line from the data points.

Is the PMOD composite correct in including this calibration glitch in the ACRIM gap or are the ACRIM and IRMB right to neglect it? As discussed by Fröhlich (2000, 2006), the ERBE data and a two-component model of TSI provide support for the inclusion of the skip in the PMOD, but a fully independent and definitive test has recently been supplied by Wenzler *et al.* (2006) from their analysis of solar magnetogram data. The spectral and total irradiance reconstructions (SATIRE) model of TSI has been developed to predict TSI from solar magnetograms (Solanki 2002; Krivova *et al.* 2003). This model characterizes each pixel of a solar magnetogram as either quiet Sun, sunspot umbra, sunspot penumbra or facular. The only free input parameter to the model is the facular pixel filling factor (faculae, unlike sunspots being smaller than the instrument pixel size). The contribution to the TSI of each pixel is then evaluated for the photospheric surface classification and the position on the disc of the pixel in question. The TSI is then quantified by summing over the entire solar disc. Figure 4 shows the scatter plot given by Krivova *et al.* (2003) of the daily TSI values for 1996–2002 derived by this method using magnetograms from the Michelson doppler imager (MDI) instrument onboard the SoHO spacecraft (Scherrer *et al.* 1995), as a function of the simultaneous TSI value observed by the VIRGO instrument (Fröhlich *et al.* 1995), also on SoHO. It can be seen that the agreement is very good: the correlation coefficient is 0.96 and the best-fit

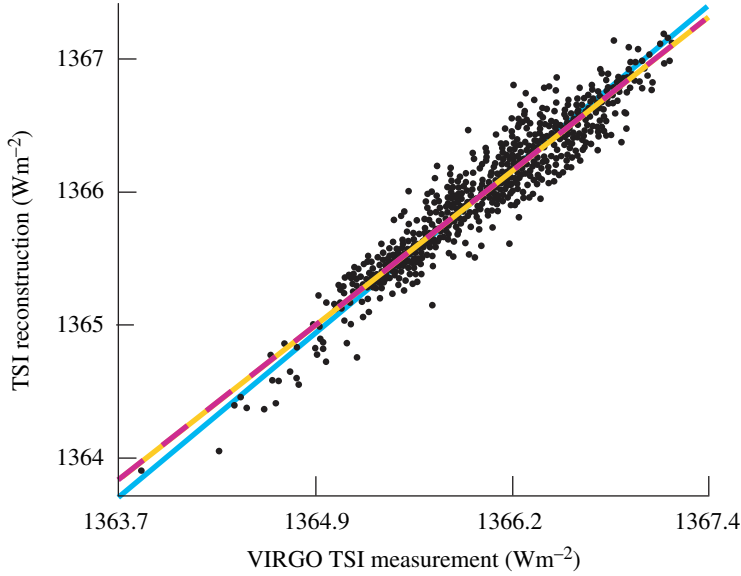


Figure 4. Scatter plot of the daily values of TSI, as simulated from SoHO MDI magnetograms using the SATIRE procedure, as a function of the simultaneous value observed by the VIRGO instrument on SoHO. The data shown are for 1996–2002 and the correlation coefficient ( $r$ ) is 0.96. The dashed mauve/orange line is the best least-squares linear regression fit and the light blue line is the ideal line of perfect agreement (adapted from [Krivova et al. 2003](#)).

linear regression (shown as the dashed mauve and orange line) is very close to the ideal (shown in light blue). This agreement is achieved with just one free fit variable in the model (the facular filling factor). Recently, [Wenzler et al. \(2006\)](#) have extended this analysis to ground-based magnetograms. This is not a trivial undertaking as additional factors, such as (partial) cloud cover, have to be corrected for. The use of ground-based data is highly significant as it extends the interval that can be studied this way back to 1976; this means that it covers the whole interval of the ACRIM and PMOD composites, including the ACRIM gap. Tests of the accuracy of the method using ground-based magnetograms against the SoHO VIRGO data show it performs with almost the same accuracy as shown in [figure 4](#) for the space-based magnetograms.

These TSI reconstructions are so accurate that they provide a good test of the TSI composites. [Figure 5](#) shows a scatter plot of the TSI, as derived from ground-based magnetograms, as a function of the PMOD composite value for the interval 1979–2003: the correlation coefficient is 0.91 and the slope  $0.978 \pm 0.008$ . One should keep in mind that the corresponding numbers for the ACRIM and IRMB composites are 0.84 and 0.87 with slopes of  $0.939 \pm 0.011$  and  $1.011 \pm 0.010$ . The light blue line is the ideal fit and the dashed blue line is the ideal minus the offset of  $0.57 \text{ W m}^{-2}$  for the second population observed in [figure 3](#). This provides a direct and independent test of the composites: if the PMOD correction at the ACRIM-gap skip is correct then the data points should be clustered around the ideal (light blue) line; if the lack-of-correction in the ACRIM composite is correct then a second population should appear aligned along the dashed blue line. [Figure 5](#) shows no such second population. Thus the modelling of [Wenzler et al. \(2006\)](#) supports the

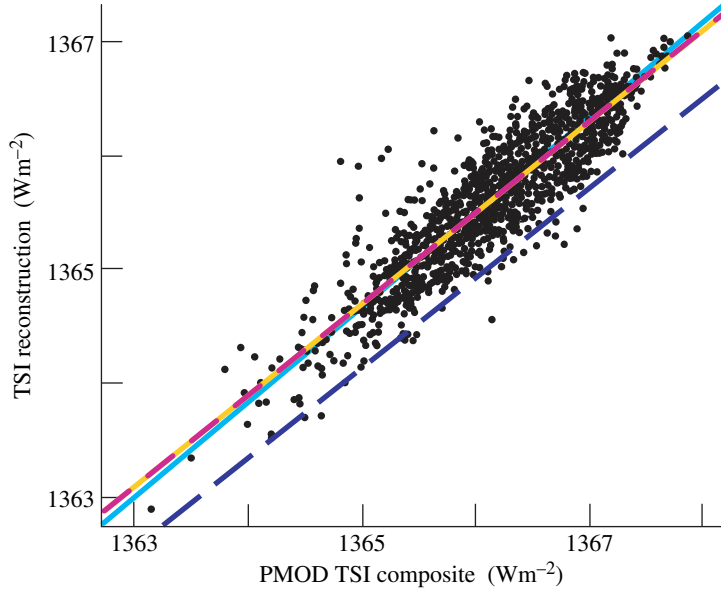


Figure 5. Scatter plot of the daily values of the TSI, as simulated from ground-based magnetograms using the SATIRE procedure, as a function of the simultaneous PMOD composite value,  $\text{TSI}_{\text{PMOD}}$ . The data shown are for 1979–2003 and the correlation coefficient ( $r$ ) is 0.91. The dashed mauve/orange line is the best least-squares linear regression fit and the light blue line is the ideal line of perfect agreement. If the skip in the PMOD composite calibration during the ACRIM gap was in error, then data from before the skip would line up along the dashed blue line, the offset being derived from figure 3 (adapted from Wenzler *et al.* (2006); for more details see T. Wenzler, PhD thesis ETH 16199, Zürich).

PMOD composite and strongly suggests that the ACRIM is an error in failing to account for the Nimbus HF pointing anomaly during the ACRIM gap. The IRMB composite is also much less reliable, due to effects mentioned previously.

To understand the implications of the difference shown in figure 2*a*, figure 6 repeats the analysis of paper 1, applying it to the ACRIM composite as well as the PMOD composite. Figure 6*e* shows that the PMOD composite gives a decline in TSI since 1985, as reported in paper 1, whereas the ACRIM composite (figure 6*d*) gives a rise up until 1996 with a subsequent fall. As we have shown, the increase arises almost entirely from the pointing direction glitch during the ACRIM gap. Comparison with figure 6*a,c* shows that the PMOD composite trend matches the trend in the sunspot number  $R$ , whereas the trend in the ACRIM composite matches that in the galactic cosmic ray (GCR) counts  $C$ . Hence, the long-term trend in the PMOD composite is consistent with its solar cycle variation, whereas that in the ACRIM composite is in the opposite direction to the solar cycle variation (since TSI peaks at sunspot maximum when the GCR flux is a minimum). The use of ACRIM therefore leads to a paradoxical, but not an impossible, situation—it is an inconsistency that would require a complex explanation, calling for two competing effects in the relationship between TSI and GCR fluxes that work in opposite directions, such that an anticorrelation between TSI and GCR fluxes dominates on time scales of the solar cycle and shorter, yet a correlation between TSI and GCR fluxes dominates on time scales longer than the solar cycle. One possibility may be related to so-called

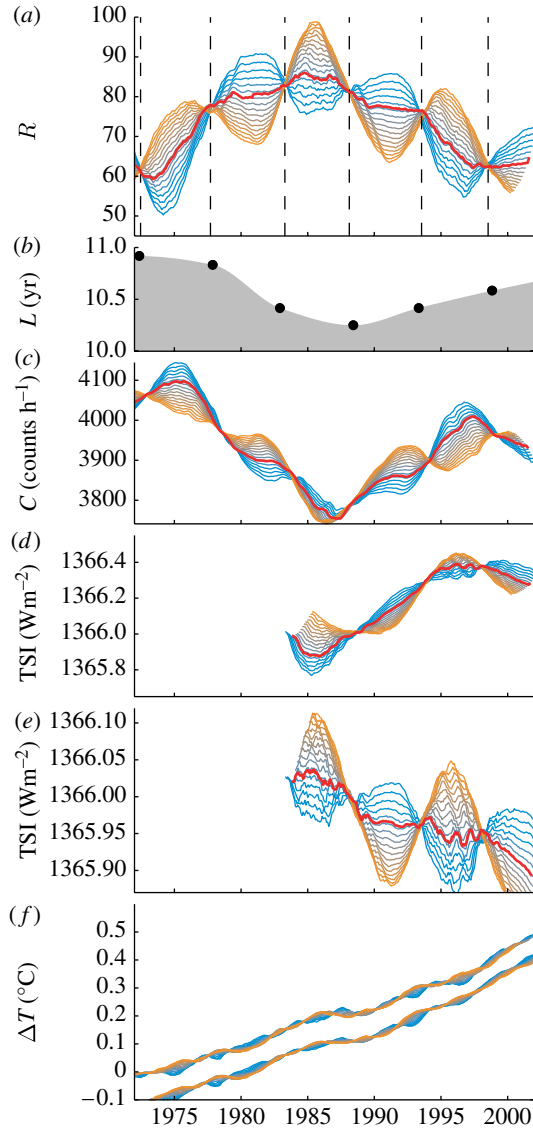


Figure 6. Running means of various parameters studied by Lockwood & Fröhlich (2007), plus of the ACRIM TSI composite. (a) the sunspot number,  $R$ ; (b) the solar cycle length,  $L$ ; (c) the Climax cosmic ray counts  $C$ ; (d) The ACRIM TSI composite,  $TSI_{\text{ACRIM}}$ ; (e) the PMOD TSI composite,  $TSI_{\text{PMOD}}$ ; and (f) the global mean surface air temperature anomaly  $\Delta T$  from the GISS and HadCRUT3 reconstructions from meteorological station and ship/buoy data. In each case, the blue to orange lines show running means over intervals  $T=[9.00: 0.25: 13.00]$ . The red line gives averages over the interpolated solar cycle length  $L$  shown by the grey shaded area in (b). The black dots in (b) show the cycle length derived from the node locations given by the vertical dashed lines in (a).

‘ephemeral’ magnetic regions in the photosphere in which Hagenaar *et al.* (2003) find flux emergence to be anticorrelated with that in active regions. Therefore, where the long-term trend in TSI is caused by a brightening effect of ephemeral flux, this could potentially explain the variation predicted by the ACRIM composite.

However, acceptance of the trend in the ACRIM composite would have profound implications. Figure 6 shows that, for this composite, the trend in TSI on time scales longer than the solar cycle is positively correlated with the GCR flux variation (the opposite to the known variation with the solar cycle) and hence this would predict a decline in TSI throughout most of the twentieth century—the opposite to almost all TSI reconstructions produced to date (e.g. Lean *et al.* 1995; Lockwood 2006). The TSI reconstructions are generally based on sunspot number (an exception is Lockwood & Stamper (1999) who used observed, but unexplained, correlations between all the individual TSI data series, thus avoiding use of a TSI composite, and the open solar magnetic flux on decadal time scales). The amplitude  $A_{\text{mm}}$  of the drift in TSI between the Maunder minimum (*ca* 1700) and recent decades was originally estimated using the observed distribution of the brightness of Sun-like stars in their chromospheric emissions. (Note that  $A_{\text{mm}}$  is defined here such that  $A_{\text{mm}} > \phi$  means that the TSI was lower in the Maunder minimum than in recent decades.) This scaling assumed that brighter Sun-like stars (of similar age and chemical abundance to the Sun) show a decadal-scale activity cycle and are analogous to the present-day Sun, whereas the less-bright stars were found to be non-cyclic and assumed to be analogous to the Sun during its Maunder minimum. The use of such stellar analogues for estimating the long-term changes in TSI was based on the work of Baliunas & Jastrow (1990), who surveyed observations of Sun-like stars and found a bimodal distribution in the ‘S-index’, which characterizes the chromospheric emissions, with the non-cyclic stars in an isolated, well-defined, low-S peak that accounted for approximately one-third of the set. Recent surveys have not reproduced this bimodal distribution and suggest that the selection of the original set was flawed (Giampapa 2004; Hall & Lockwood 2004). Furthermore, although non-cyclic stars were again found to be about one-third of the total, they were present throughout the distribution, not just at low-S values. More recent reconstructions have scaled down the estimated  $A_{\text{mm}}$  but it has remained positive (see review by Lockwood 2006). Extrapolating the long-term drift in TSI required by the ACRIM composite would imply that non-cyclic stars were actually brighter than the cyclic ones and that  $A_{\text{mm}}$  was negative (i.e. the Sun was brighter in the Maunder minimum than now). Note also that the trend in the ACRIM composite on time scales greater than the solar cycle is also exactly the opposite to what is assumed in palaeoclimate studies that employ cosmogenic isotopes generated by cosmic ray bombardment of the atmosphere as an inversely correlated proxy for TSI (e.g. Bond *et al.* 2001; Neff *et al.* 2001).

Almost all of the evidence for solar effects on climate on time scales larger than the solar cycle (using both data from the network of weather stations, ships and buoys for the past 150 years and from proxies, such as from tree rings, for earlier times) is based on the idea that  $A_{\text{mm}}$  is positive. (e.g. the Maunder minimum is usually associated with the ‘little ice age’ in Europe). Hence, all this evidence would need to be rejected if the long-term drift in the ACRIM composite was correct.

However, this discussion is largely hypothetical, given that Wenzler *et al.* (2006) show us that the trend in the PMOD composite is almost certainly correct and that in the ACRIM is not. An independent analysis of ERBE data gives the same conclusion, as does comparison with a model based on sunspot darkening and chromospheric plages as a proxy for facular and network brightening (Fröhlich 2000, 2006).

### 3. The effect of smoothing time constant

In [paper 1](#), the solar cycle variations were smoothed out to reveal long-term trends. The actual response time of the climate system  $\tau$  is set by the thermal response time of the upper ocean layers and, hence, the time constant estimated depends on the depth to which a variation penetrates and hence the heat capacity of the relevant upper ocean layer. Estimates have varied from less than 1 year to several decades ([Wigley & Raper 1990](#); [Douglass \*et al.\* 2004](#); [Schwartz 2007](#)). We know that in the Earth's climate system, solar cycle variations are not completely smoothed out ([paper 3](#)) and it has been suggested that the conclusions of [paper 1](#) are somehow undermined by this ([D'Aleo 2007](#); [Svensmark & Friis-Christensen 2007](#)). The solar cycle variations have been detected in mean global surface air temperatures ([Douglass \*et al.\* 2004](#); [Lean 2006](#)), ocean surface temperatures ([White \*et al.\* 1997](#)) and tropospheric temperatures ([Labitze & van Loon 1995](#); [Christy \*et al.\* 2000](#); [Svensmark & Friis-Christensen 2007](#)) and are expected from climate model simulations ([Santer \*et al.\* 2001](#)). In this section, we show that allowing for response times short enough to allow solar cycle variations not to be completely damped makes no difference to the conclusions of [paper 1](#). To enable this, in the next section we construct a splined GCR flux variation extending back to 1900 by combining extrapolated values with measurements since 1953. The TSI reconstructions of, for example, [Lean \*et al.\* \(1995\)](#) and [Lockwood \(2006\)](#) give a consistent, monotonic (inverse) relationship between TSI and GCR fluxes on all time scales between years and centuries. This being the case, conclusions drawn using the GCR reconstruction waveform derived here can be applied to TSI, as well as GCR, variations.

#### (a) *Reconstruction of century-scale GCR variation*

Cosmic ray measurements by neutron monitors extend back to 1953 in the case of the Climax and the Huancayo/Haleakala observatories. The Earth's geomagnetic field deflects GCRs and sets a lower ('cut-off') limit to the 'rigidity' of GCRs that can be detected at a given geomagnetic latitude. Rigidity is a measure of the tendency of the GCR to move in a straight line and is measured in GV. The neutron monitors in Huancayo, Peru and Haleakala, Hawaii provide a continuous and homogeneous data sequence, with the data series being continued at the equivalent site at Haleakala, Hawaii (at the same altitude and geomagnetic latitude) after monitoring ceased at Huancayo, Peru in 1993 ([Shea & Smart 2004](#)). For these stations, primary cosmic rays of rigidity exceeding a geomagnetic cut-off of 13.5 GV are detected; for the higher latitude Climax station the threshold is 3.0 GV. Prior to the commissioning of these stations, there are measurements from ground-based ionization chambers ([Forbush 1954, 1958](#)) and also from balloon flights ([Neher 1967](#)). The Neher data are particularly important as they were carried out to very high precision and reveal a downward trend in cosmic ray fluxes in the twentieth century ([McCracken & Beer 2007](#)).

The open solar magnetic flux (the 'coronal source flux') anticorrelates very well with the GCR fluxes seen by neutron monitors over recent solar cycles ([Rouillard & Lockwood 2004](#)); [fig. 3 of paper 1](#) shows that this anticorrelation is valid for the drift over several decades as well as for the solar cycle, as do the

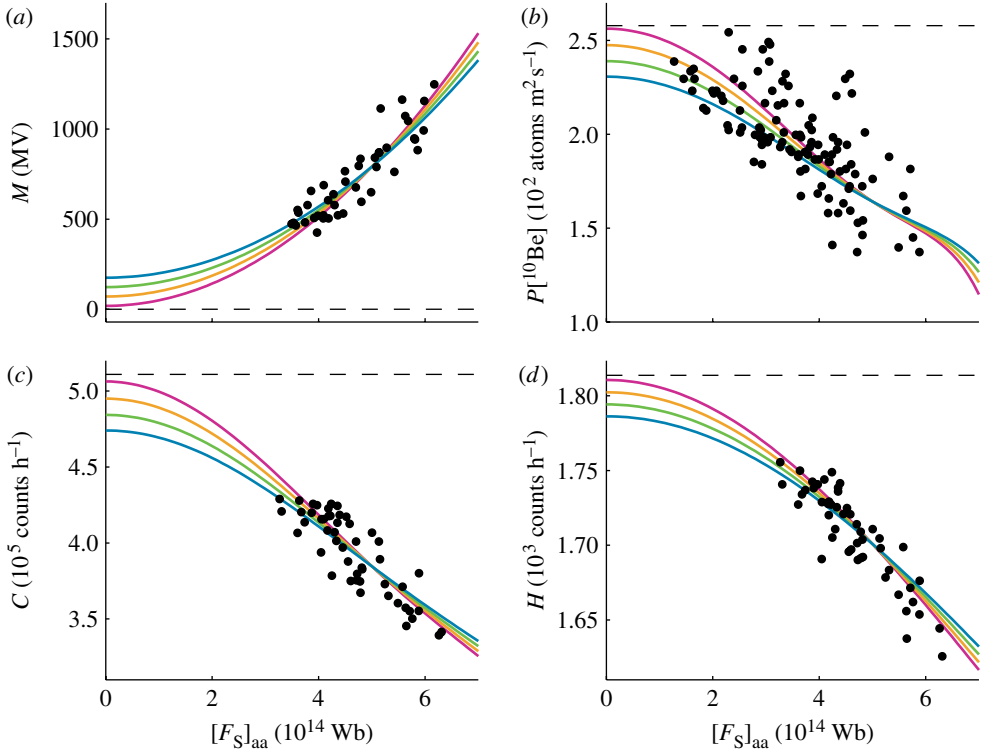


Figure 7. Scatter plots of annual means the open solar flux derived from geomagnetic activity,  $[F_S]_{aa}$  against: (a) the heliospheric modulation parameter,  $M$ ; (b) the production rate of the  $^{10}\text{Be}$  cosmogenic isotope,  $P[^{10}\text{Be}]$ ; (c) the Climax neutron monitor counts  $C$  (sensitive to cosmic rays of rigidity greater than 3 GV); (d) the Huancauyo/Hawaii neutron monitor counts  $H$  (sensitive to cosmic rays of rigidity greater than 13 GV). In each panel the dots are data points and the dashed horizontal line is the estimated value for the local interstellar spectrum (LIS) and the mauve, orange, green and blue lines are theoretical curves from GEANT-4 simulations for assumed values of  $M$  at the end of the Maunder minimum,  $M_{mm}$ , of 50, 100, 150 and 200 MV, respectively. In the case of  $P[^{10}\text{Be}]$ , the data points shown are scaled from the abundance of  $^{10}\text{Be}$  found in the Dye-3 Greenland ice core.

analyses of Usoskin *et al.* (2002) and McCracken (2007). Lockwood (2001) extrapolated the GCR fluxes using the open solar flux,  $[F_S]_{aa}$  derived from geomagnetic activity (Lockwood *et al.* 1999; Rouillard *et al.* 2007) by assuming a linear relationship but, as pointed out by Mursula *et al.* (2003), the relationship will not be linear if  $[F_S]_{aa}$  is low, such that the GCR flux approaches its maximum, which is that in the local interstellar medium.

Figure 7 shows an analysis of the relationship of  $[F_S]_{aa}$  to various cosmic ray observations. Figure 7a shows the heliospheric modulation parameter  $M$ , derived by Masarik & Beer (1999) by fitting the annual mean counts detected by the Deep River neutron monitor (at sufficiently high latitudes that it is sensitive to GCRs of rigidity greater than 1 GV, limited by the atmosphere rather than the geomagnetic field). The modulation parameter is a simple way of characterizing the shielding effect of the heliosphere on GCR fluxes at Earth (Bonino *et al.* 2001; Usoskin *et al.* 2005);  $M$  of zero gives the interstellar GCR spectrum, whereas the largest derived annual mean

of  $M$  is 1250 MV, which fits the mean spectrum observed in 1959, at the peak of the largest solar cycle observed to date. (Note that for monthly mean data,  $M$  of 2250 MV has been derived by Usokin *et al.* (2005).) In order to simulate neutron counts, Masarik & Beer used GEANT-4/MCNP simulations of the effects of the GCR spectrum (for a given  $M$ ) impacting the Earth's atmosphere. The GEANT-4 and MCNP simulation codes allow particle production and transport calculations with no free parameters (Brun *et al.* 1987; Briesmeister 1993). The four curves shown are fitted quadratics in  $[F_S]_{\text{aa}}$  constrained by four assumed values of  $M$  at the end of the Maunder minimum,  $M_{\text{mm}}$ . The corresponding value of  $[F_S]_{\text{aa}}$  at the end of the Maunder minimum is taken to be  $1 \times 10^{14}$  Wb, which was derived by Lockwood (2003) by running the model of Solanki *et al.* (2000) backwards in time from a starting point of the total open solar flux observed by Ulysses during its first perihelion fast latitude scan in 1996–1997. In this model, the emergence rate of open flux is derived from the sunspot number. From these fitted  $[F_S]_{\text{aa}} - M$  curves, the results of the GEANT-4 simulations of Masarik & Beer are used to give the variation with  $[F_S]_{\text{aa}}$  of the global production rate of the  $^{10}\text{Be}$  cosmogenic isotope,  $P[^{10}\text{Be}]$  (figure 7b); the counts  $C$  detected by the Climax neutron monitor, sensitive to GCRs of rigidity greater than 3 GV (figure 7c); and the counts  $H$  detected by the Huancayo/Hawaii neutron monitors, sensitive to GCRs of rigidity greater than 13 GV (figure 7d). In figure 7c,d, the data points are observed annual mean count rates, plotted as a function of the corresponding annual mean  $[F_S]_{\text{aa}}$  values. In figure 7b, the abundance of the  $^{10}\text{Be}$  cosmogenic isotope from the Dye-3 ice core is plotted (Beer *et al.* 1998, 2006). All four panels show that the  $[F_S]_{\text{aa}}$  varies monotonically with the GCR indicator—the scatter is highest for the  $^{10}\text{Be}$  cosmogenic isotope data, partly due to dating uncertainties. It can be seen that these are not completely linear variations, as at low  $[F_S]_{\text{aa}}$  the curve asymptotically approaches the local interstellar spectrum value. The variation giving the best least-squares fit to  $C$  in figure 7c is that for  $M_{\text{mm}} = 100$  MV. Using the curve for  $M_{\text{mm}} = 100$  MV and the variation of  $[F_S]_{\text{aa}}$  given by Rouillard *et al.* (2007), the count rates seen at Climax can be extrapolated back to before the start of the observations. A spline of these extrapolated values (before 1953), from a linear regression fit to the observed values after 1953, is given in figure 8. This variation is consistent with the data of Forbush (1954) and Neher (1967) and is very similar to that derived using different methods by Rouillard & Lockwood (2007), Usoskin *et al.* (2002) and McCracken & Beer (2007).

(b) *Effect of terrestrial response time constant*

In order to simulate the effects of possible response times to the solar variation implied by the reconstructed GCR flux in figure 8, we pass the data through a simple low-pass ‘RC’ filter giving a response time constant  $\tau$  that is varied between 1 and 10 years in steps of 1 year. The actual climate system, of course, has a wide variety of response time scales, ranging from hours to centuries (the latter for deep oceanic circulation) and the simple, single exponential used here is an approximation to the convolution of all the real responses. The results are shown by the coloured lines in figure 8. As expected, the larger the value of  $\tau$ , the more the solar cycle variation is smoothed out and the response is delayed. These smoothed variations are then fitted individually using linear least-squares regression to the HadCRUT3 global mean surface temperature anomaly data (Brohan *et al.* 2006). This temperature

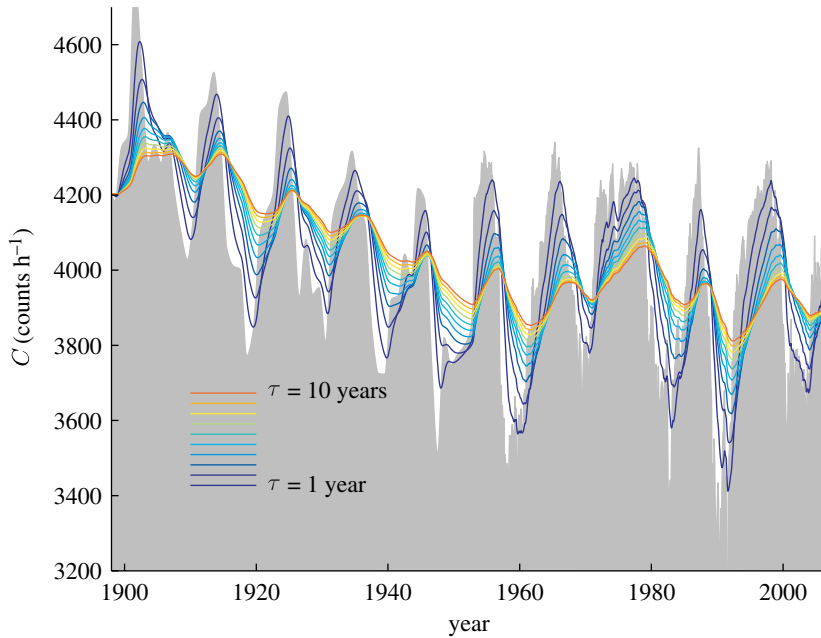


Figure 8. Grey area: the observed and extrapolated cosmic ray counts  $C$  at the Climax neutron monitor site. The observations made from 1953 to the present day are extrapolated back in time using the open solar flux from geomagnetic activity,  $[F_S]_{aa}$  and the variation shown in figure 7c for  $M_{min}=100$  MV (see text for details). Coloured lines: the observed and extrapolated  $C$  values, passed through a low-pass filter giving a response time  $\tau$  that is varied between 1 year (dark blue line) and 10 years (red line) in steps of 1 year.

reconstruction is generated by the UK Meteorological Office and the Climate Research Unit at The University of East Anglia using land surface air temperature observations from more than 4000 weather stations and sea surface temperature from ships and buoys. The results are shown in figure 9. The slope of the regressions is negative, showing that any correlation would imply lower cosmic ray flux is associated with higher air surface temperatures. It can be seen that reasonable fits to the trend, and to some extent to the decadal-scale variations, can be obtained for the data before *ca* 1990, but that since then none of the variations explain the observed trend at all. The conclusion of paper 1 that the trend in solar forcing has been in the wrong direction since *ca* 1987 is not influenced by the choice of thermal time constant for smoothing the decadal-scale solar variations. Figures 8 and 9 have used the observed and extrapolated cosmic ray fluxes, but because there is a strong anticorrelation between cosmic rays and TSI reconstructions (Lean *et al.* 1995; Lockwood 2006), the same conclusion is reached if we used a spline of the PMOD TSI observation composite with a reconstruction before the start of such observations.

#### 4. Conclusions

We have reviewed the difference between the ACRIM, IRMB and PMOD TSI composites and shown that the upward trend in the ACRIM before 1996 (after which it is downward), compared with the downward trend since 1985 in the

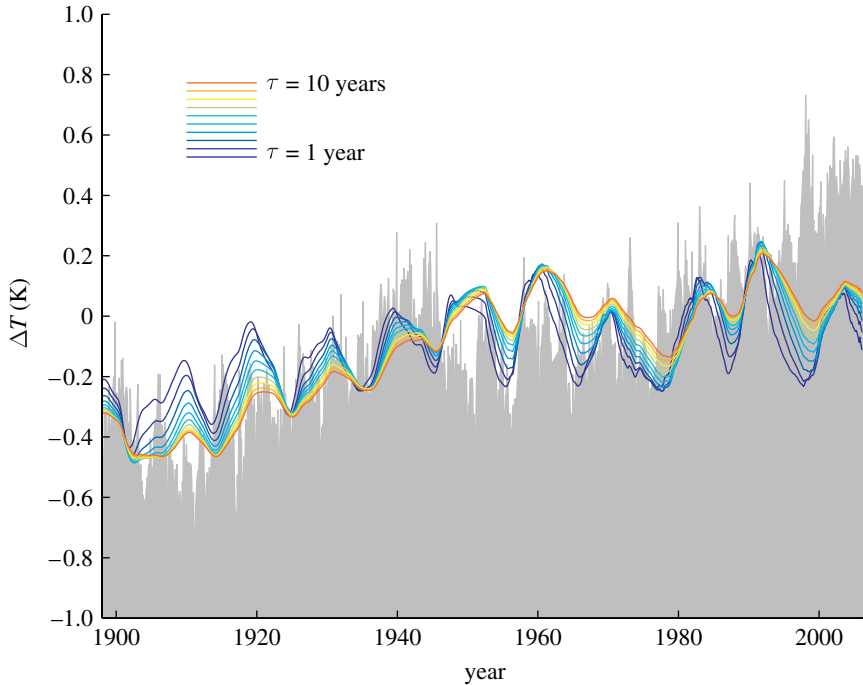


Figure 9. Grey shaded area: the global mean surface air temperature anomaly  $\Delta T$  from the HadCRUT3 compilation of meteorological station and ship/buoy data. Coloured lines: the best least-squares fits of the low-pass filtered variations shown in figure 8, using the same colours (so  $\tau = 1$  year for the dark blue line and 10 years for the red line). Because  $C$  and  $\Delta T$  are broadly anticorrelated, the best-fit variations are inverted compared to the original variations in figure 8.

PMOD composite, is due to a calibration glitch in the Nimbus-7 HF data during the ACRIM gap, which is allowed for in the PMOD composites, but not the ACRIM. Fröhlich (2006) has shown that the PMOD composite is consistent with the independent, but relatively noisy, ERBE data, whereas the ACRIM and IRMB are not. Here, we point out that the TSI modelling of Wenzler *et al.* (2006) from ground-based magnetograms is also consistent with the PMOD composite and inconsistent with ACRIM and IRMB. The great accuracy of this modelling, and the fact that the facular filling factor is the only free parameter, means that it provides an excellent test. In addition, we point out that the ACRIM composite generates some curious phenomena that would need explanation. For example, if the ACRIM composite were to be correct, the strong negative correlation between TSI and GCR fluxes over the solar cycle, for which we have a physical explanation, would reverse polarity on longer time scales for reasons we do not yet understand. This would invalidate almost all previous evidence for solar effects on climate on time scales longer than the solar cycle.

We have also shown that the effect of smoothing time constant cannot be a possible source of the divergent trends in air surface temperature and solar inputs described in paper 1. Hence, like many authors before us, we conclude there is no credible way that the recent rise in air surface temperature can be attributed to solar effects. As in paper 1, Lockwood *et al.* (1999) and Solanki & Krivova (2003), we have not drawn on complex general circulation climate models to draw this conclusion.

The authors are grateful to the World Data Centre system and the many scientists who contribute data to it. Thanks are extended to the VIRGO and SoHO teams; SoHO is a cooperative ESA/NASA mission launched in late 1995. The work of ML at the Rutherford Appleton Laboratory is funded by the UK Science and Technology Facilities Council.

## References

- Baliunas, S. & Jastrow, R. 1990 Evidence for long-term brightness changes of solar-type stars. *Nature* **348**, 520–523. (doi:10.1038/348520a0)
- Beer, J., Tobias, S. & Weiss, N. 1998 An active Sun throughout the Maunder minimum. *Sol. Phys.* **181**, 237–249. (doi:10.1023/A:1005026001784)
- Beer, J., Vonmoos, M. & Mischeler, R. 2006 Solar variability over the past several millennia. *Space Sci. Rev.* **125**, 67–79. (doi: 10.1007/s11214-006-9047-4)
- Bond, G. *et al.* 2001 Persistent solar influence on North Atlantic climate during the Holocene. *Science* **294**, 2130–2136. (doi:10.1126/science.1065680)
- Bonino, G., Cini-Castagnoli, G., Cane, D., Taricco, C. & Bandahri, N. 2001 Solar modulation of the galactic cosmic ray spectra since the Maunder minimum. In *Proc. Int. Cosmic Ray Conf.*, vol. 27 (ed. R. Schlickeiser), pp. 3769–3772. Copernicus Gesellschaft, Katlenburg-Lindau, Germany.
- Briesmeister, J. F. 1993 MCNP—a general Monte Carlo *N*-particle transport code, version 4A. Report no. LA-12625-M, Los Alamos National Laboratory, NM.
- Brohan, P., Kennedy, J. J., Haris, I., Tett, S. F. B. & Jones, P. D. 2006 Uncertainty estimates in regional and global observed temperature changes: a new dataset from 1850. *J. Geophys. Res.* **111**, D12 106. (doi:10.1029/2005JD006548)
- Brun, R., Bruyant, F., Maire, M., McPherson, A. C. & Zanarini, P. 1987 *GEANT3 user's guide*. Report DD/EE/84-1, European Organization for Nuclear Research, Geneva, Switzerland.
- Chapman, G. A., Cookson, A. M. & Dobias, J. J. 1996 Variations in total solar irradiance during solar cycle 22. *J. Geophys. Res.* **101**, 13 541–13 548. (doi:10.1029/96JA00683)
- Christy, J. R., Spencer, R. W. & Braswell, W. D. 2000 MSU tropospheric temperatures: dataset construction and radiosonde comparisons. *J. Atmos. Oceanic Tech.* **17**, 1153–1170. (doi:10.1175/1520-0426(2000)017<1153:MTTDC>2.0.CO;2)
- Crommelynck, D., Fichot, A., Lee III, R. B. & Romero, J. 1995 First realisation of the space absolute radiometric reference (SARR) during the ATLAS 2 flight period. *Adv. Space Res.* **16**, 17–23. (doi:10.1016/0273-1177(95)00261-C)
- D'Aleo, J. 2007 Shining more light on the solar factor: a discussion of problems with the Royal Society paper by Lockwood and Fröhlich. See Science and Public Policy Unit website, [http://scienceandpublicpolicy.org/sppi\\_originals/shining\\_more\\_light\\_on\\_the\\_solar\\_factor\\_a\\_discussion\\_of\\_problems\\_with\\_the\\_royal\\_society.html](http://scienceandpublicpolicy.org/sppi_originals/shining_more_light_on_the_solar_factor_a_discussion_of_problems_with_the_royal_society.html).
- Dewitte, S., Crommelynck, D., Mekaoui, S. & Joukoff, A. 2004 Measurement and uncertainty of the long-term total solar irradiance trend. *Sol. Phys.* **224**, 209–216. (doi:10.1007/s11207-005-5698-7)
- Douglass, D. H., Clader, B. D. & Knox, R. S. 2004 Climate sensitivity of Earth to solar irradiance: update. Paper presented at *2004 Solar Radiation and Climate (SORCE) meeting on Decade Variability in the Sun and the Climate, Meredith, New Hampshire, 27–29 October 2004*.
- Forbush, S. E. 1954 World-wide cosmic ray variations, 1937–1952. *J. Geophys. Res.* **59**, 525–542. (doi:10.1029/JZ059i004p00525)
- Forbush, S. E. 1958 Cosmic ray intensity variations during two solar cycles. *J. Geophys. Res.* **63**, 651–669. (doi:10.1029/JZ063i004p00651)
- Fröhlich, C. 2000 Observations of irradiance variations. *Space Sci. Rev.* **94**, 15–24. (doi:10.1023/A:1026765712084)
- Fröhlich, C. 2003 Long-term behaviour of space radiometers. *Metrologia* **40**, 60–65. (doi:10.1088/0026-1394/40/1/314)
- Fröhlich, C. 2006 Solar irradiance variability since 1978: revision of the PMOD composite during solar cycle 21. *Space Sci. Rev.* **125**, 53–65. (doi:10.1007/s11214-006-9046-5)

- Fröhlich, C. & Lean, J. 1998 The Sun's total irradiance: cycles, trends and related climate change uncertainties since 1978. *Geophys. Res. Lett.* **25**, 4377–4380. (doi:10.1029/1998GL900157)
- Fröhlich, C. & Lean, J. 2004 Solar radiative output and its variability: evidence and mechanisms. *Astron. Astrophys. Rev.* **12**, 273–320. (doi: 10.1007/s00159-004-0024-1)
- Fröhlich, C. *et al.* 1995 VIRGO: experiment for helioseismology and solar irradiance monitoring. *Sol. Phys.* **162**, 101–128. (doi:10.1007/BF00733428)
- Giampapa, M. 2004 Stellar analogs of solar activity: the Sun in a stellar context. In *The Sun, solar analogs and the climate*, vol. 34 (eds I. Redi, M. Güdel & W. Schmutz). Proc. Saas-Fee advanced course. Berlin, Germany; New York, NY: Springer.
- Hagenaar, H. J., Schrijver, C. J. & Title, A. M. 2003 The properties of small magnetic regions on the solar surface and the implications for the solar dynamo. *Astrophys. J.* **584**, 1107–1119. (doi:10.1086/345792)
- Hall, J. C. & Lockwood, G. W. 2004 The chromospheric activity and variability of cycling and flat activity solar-analog stars. *Astrophys. J.* **614**, 942–946. (doi:10.1086/423926)
- Kerr, R. 1997 Did satellites spot a brightening Sun? *Science* **277**, 1923–1924. (doi:10.1126/science.277.5334.1923)
- Krivova, N. A., Solanki, S. K., Fligge, M. & Unruh, Y. C. 2003 Reconstruction of solar irradiance variations in cycle 23: is solar surface magnetism the cause? *Astron. Astrophys.* **399**, L1–L4. (doi:10.1051/0004-6361:20030029)
- Labitze, K. & van Loon, H. 1995 Signal of the 11-year sunspot cycle in the upper troposphere–lower stratosphere. *Space Sci. Rev.* **80**, 393–410. (doi:10.1023/A:1004907126955)
- Lean, J. 2006 Comment on ‘Estimated solar contribution to the global surface warming using the ACRIM TSI satellite composite’ by N. Scafetta and B. J. West. *Geophys. Res. Lett.* **33**, L15 701. (doi:10.1029/2005GL025342)
- Lean, J., Beer, J. & Bradley, R. 1995 Reconstruction of solar irradiance since 1610: implications for climate change. *Geophys. Res. Lett.* **22**, 3195–3319. (doi:10.1029/95GL03093)
- Lee III, R. B., Gibson, M. A., Wilson, R. S. & Thomas, S. 1995 Long-term total solar irradiance variability during sunspot cycle 22. *J. Geophys. Res.* **100**, 1667–1675. (doi:10.1029/94JA02897)
- Lockwood, M. 2001 Long-term variations in the magnetic fields of the Sun and the heliosphere: their origin, effects and implications. *J. Geophys. Res.* **106**, 16 021–16 038. (doi:10.1029/2000JA000115)
- Lockwood, M. 2003 Twenty-three cycles of changing open solar magnetic flux. *J. Geophys. Res.* **108**, 1128. (doi:10.1029/2002JA009431)
- Lockwood, M. 2006 What do cosmogenic isotopes tell us about past solar forcing of climate? *Space Sci. Rev.* **125**, 95–109. (doi:10.1007/s11214-006-9049-2)
- Lockwood, M. In press. Recent changes in solar outputs and the global mean surface temperature. III. Analysis of contributions to global mean air surface temperature rise. *Proc. R. Soc. A* (doi:10.1098/rspa.2007.0348)
- Lockwood, M. & Fröhlich, C. 2007 Recent oppositely-directed trends in solar climate forcings and the global mean surface air temperature. *Proc. R. Soc. A* **463**, 2447–2460. (doi:10.1098/rspa.2007.1880)
- Lockwood, M. & Stamper, R. 1999 Long-term drift of the coronal source magnetic flux and the total solar irradiance. *Geophys. Res. Lett.* **26**, 2461–2464. (doi:10.1029/1999GL900485)
- Lockwood, M., Stamper, R., Wild, M. N., Balogh, A. & Jones, G. 1999 Our changing Sun. *Astron. & Geophys.* **40**, 4.10–4.16.
- Masarik, J. & Beer, J. 1999 Simulation of particle fluxes and cosmogenic nuclide production in the Earth's atmosphere. *J. Geophys. Res.* **104**, 12 099–12 112. (doi:10.1029/1998JD200091)
- McCracken, K. G. 2007 Heliomagnetic field near Earth, 1428–2005. *J. Geophys. Res.* **112**, A09 106. (doi:10.1029/2006JA012119)
- McCracken, K. G. & Beer, J. 2007 Long-term changes in the cosmic ray intensity at Earth, 1428–2005. *J. Geophys. Res.* **112**, A10 101. (doi:10.1029/2006JA012117)
- Mursula, K., Usoskin, I. G. & Kovaltsov, G. A. 2003 Reconstructing the long-term cosmic ray intensity: linear relations do not work. *Ann. Geophys.* **21**, 863–867.

- Neff, U., Burns, S. J., Mangini, A., Mudelsee, M., Fleitmann, D. & Matter, A. 2001 Strong coherence between solar variability and the monsoon in Oman between 9 and 6 kyr ago. *Nature* **411**, 290–293. (doi:10.1038/35077048)
- Neher, H. V. 1967 Cosmic ray particles that changed from 1954 to 1958 to 1965. *J. Geophys. Res.* **72**, 1527–1539.
- Rouillard, A. P. & Lockwood, M. 2004 Oscillations in the open solar magnetic flux with period 1.68 years: imprint on galactic cosmic rays and implications for heliospheric shielding. *Ann. Geophys.* **22**, 4381–4396.
- Rouillard, A. P. & Lockwood, M. 2007 Centennial changes in solar activity and the response of galactic cosmic rays. *Adv. Space Res.* **40**, 1078–1086. (doi:10.1016/j.asr.2007.02.096)
- Rouillard, A. P., Lockwood, M. & Finch, I. 2007 Centennial changes in the solar wind speed and in the open solar flux. *J. Geophys. Res.* **112**, A05 103. (doi:10.1029/2006JA012130)
- Santer, B. D. *et al.* 2001 Accounting for the effects of volcanoes and ENSO in comparisons of modeled and observed temperature trends. *J. Geophys. Res.* **106**, 28 033–28 059. (doi:10.1029/2000JD000189)
- Scafetta, N. & West, B. J. 2003 Solar flare intermittency and the Earth's temperature anomalies. *Phys. Rev. Lett.* **90**, 248 701–248 704. (doi:10.1103/PhysRevLett.90.248701)
- Scafetta, N. & West, B. J. 2006 Phenomenological solar contribution to the 1900–2000 global surface warming. *Geophys. Res. Lett.* **33**, L05 708. (doi:10.1029/2005GL025539)
- Scherrer, P. H. *et al.* 1995 The solar oscillations investigation—Michelson doppler imager. *Sol. Phys.* **162**, 129–188. (doi:10.1007/BF00733429)
- Schwartz, S. E. 2007 Heat capacity, time constant, and sensitivity of Earth's climate system, *J. Geophys. Res.* **112**, D24S05. (doi:10.1029/2007JD008746)
- Shea, M. A. & Smart, D. F. 2004 Fifty years of cosmic radiation data. *Space Sci. Rev.* **93**, 229–262. (doi:10.1023/A:1026500713452)
- Solanki, S. K. 2002 Solar variability and climate change: is there a link? *Astron. Geophys.* **43**, 5.9–5.13. (doi:10.1046/j.1468-4004.2002.43509.x)
- Solanki, S. K. & Krivova, N. A. 2003 Can solar variability explain global warming since 1970? *J. Geophys. Res.* **108**, 1200. (doi:10.1029/2002JA009753)
- Solanki, S. K., Schüssler, M. & Fligge, M. 2000 Secular evolution of the Sun's magnetic field since the Maunder minimum. *Nature* **480**, 445–446. (doi:10.1038/35044027)
- Svensmark, H. & Friis-Christensen, E. 2007 Reply to Lockwood and Fröhlich—the persistent role of the Sun in climate forcing. Scientific report no. 3/2007, Danish National Space Center. See [http://spacecenter.dk/publications/scientific-report-series/Scient\\_No.\\_3.pdf/view](http://spacecenter.dk/publications/scientific-report-series/Scient_No._3.pdf/view).
- Usoskin, I. G., Mursula, K., Solanki, S. K., Schüssler, M. & Kovaltsov, G. A. 2002 A physical reconstruction of cosmic ray intensity since 1610. *J. Geophys. Res.* **107**, 1374. (doi:10.1029/2002JA009343)
- Usoskin, I. G., Alanko-Huotari, K., Kovaltsov, G. A. & Mursula, K. 2005 Heliospheric modulation of cosmic rays: monthly reconstruction for 1951–2004. *J. Geophys. Res.* **110**, A12 108. (doi:10.1029/2005JA011250)
- Wenzler, T., Solanki, S. K., Krivova, N. A., Fröhlich, C. 2006 Reconstruction of solar irradiance variations in cycles 21–23 based on surface magnetic fields. *Astron. Astrophys.* **460**, 583–595. (For more details see also Wenzler, T. 2005 PhD thesis, ETH Nr 16199, Zürich.) (doi:10.1051/0004-6361:20065752)
- White, W. B., Lean, J. & Cayan, D. 1997 A response of global upper ocean temperature to changing solar irradiance. *J. Geophys. Res.* **102**, 3255–3266. (doi:10.1029/96JC03549)
- Wigley, T. M. L. & Raper, S. C. B. 1990 Climatic change due to solar irradiance changes. *Geophys. Res. Lett.* **17**, 2169–2172. (doi:10.1029/GL017i012p02169)
- Willson, R. C. 1997 Total solar irradiance trend during solar cycles 21 and 22. *Science* **277**, 1963–1965. (doi:10.1126/science.277.5334.1963)
- Willson, R. C. & Mordvinov, A. V. 2003 Secular total solar irradiance trend during solar cycles 21–23. *Geophys. Res. Lett.* **30**, 1199–1202. (doi:10.1029/2002GL016038)